Solid Earth
Discussions

Open Access

EGU

Recent developments in neutron imaging with applications for porous media research

A. P. Kaestner[1], P. Trtik[1], M. Zarebandkouki[2], D. Kazantsev[3,4], M. Snehota[5],
K. J. Dobson[6], and E. H. Lehmann[1]

[1]Laboratory for Neutron Scattering and Imaging, Paul Scherrer Institut, Villigen, Switzerland
[2]Division of Soil Hydrology, University of Goettingen, Göttingen, Germany
[3]Manchester X-Ray Imaging Facility, School of Materials, University of Manchester, Manchester, UK
[4]Manchester X-Ray Imaging Facility, Research Complex at Harwell, Didcot, UK
[5]Faculty of Civil Engineering, Czech Technical University in Prague, Prague, Czech Republic
[6]Department of Earth and Environmental Sciences, University of Munich, Munich, Germany

Discussion Paper | Discussion Paper | Discussion Paper | Discussion Paper

SED
7, 3481–3510, 2015

Neutron imaging for porous media

A. Kaestner et al.

Title Page

Abstract | Introduction
Conclusions | References
Tables | Figures

◀ | ▶

◀ | ▶

Back | Close

Full Screen / Esc

Printer-friendly Version

Interactive Discussion

Abstract

Computed tomography has become a standard method to probe processes in porous media. Neutrons enabled us to better study the dynamics of hydrogeneous fluids in the matrix of dense and opaque materials. We review recent instrumentation and method improvements to the neutron imaging facilities NEUTRA and ICON at Paul Scherrer Institute. The improvements give us higher spatial resolution making it possible to follow finer details and faster acquisition to increase the CT volume capture rate. The combination with new reconstruction techniques improve the information output with less acquired projection data and hence providing higher volume rates. Bi-modality is a further option to provide more information about the sample and the processes taking place. These features make new neutron imaging experiments to investigate the fluid distribution in porous samples possible. We demonstrate the performance on a selection of experiments performed at our neutron imaging instruments.

1 Introduction

The knowledge of how water is displaced within a sample is central to many porous media experiments, and 3-D imaging has proven to be a useful tool since it can provide high-contrast information about the displacements of fluids as well as the structures within the observed sample. Imaging can use many modalities and X-rays (XCT) are mostly used for this purpose due to the high spatial and temporal resolution that can be achieved at modern synchrotron and laboratory X-ray sources (e.g. Dobson et al. this issue), and the relative availability of X-ray CT systems. However, neutron imaging has also proven very useful for in situ studies. Neutron imaging is generally less accessible due to the small number of neutron imaging facilities worldwide, and while it cannot always compete with X-ray imaging for speed because of the available flux of most neutron sources, its advantage lies in the excellent fluid-matrix contrast arising from the high sensitivity to hydrogen. Using neutron imaging (radiography and tomography)

it is possible to quantify very small amounts of a fluid, even when the pore space itself cannot be resolved. This is in particular relevant for investigations of water displacement in bulk samples when the detailed structure of the pore space is less relevant for the understanding the fluid processes.

Another unique feature of neutron imaging is isotope sensitivity; which gives almost an order of magnitude in contrast between hydrogen (^{1}H) and deuterium (^{2}H or D). This difference allows the isotopes to be used as tracers to follow an individual pulse of water through a preconditioned porous medium to trace mixing behaviour of fluids of rather similar viscosity (Zarebanadkouki et al., 2012).

Futhermore, most metals are also less opaque to neutrons than fluids, meaning it possible to observe fluid flow in-situ within pressure and/or high temperature vessels. The flexibility of the instrumentation at neutron imaging beamlines makes it possible to meet the meet the needs of a wide user community. Some users may focus on larger samples and are less interested in the detailed information, other users need higher spatial or temporal resolution or even both. On-going instrument development steadily pushes the frontiers and makes new experiments possible. Here, we review recent advances in spatial and temporal performance for the neutron imaging instruments NEUTRA (Lehmann et al., 2001), ICON (Kaestner et al., 2011a), and BOA (Morgano et al., 2014) at the Swiss spallation Neutron Source (SINQ), Paul Scherrer Institut (PSI), and provide a collection of examples to demonstrate state of the art of neutron imaging methods. The presented instrument features are available in the ordinary user programme and can be provided on demand.

2 Methods and applications

Neutron imaging is a method that acquires radiographs representing the neutrons that were transmitted through the sample. The mechanism that prevents the neutrons from reaching the detector is a mix between absorption and scattering. Scattering is often the dominant component of the neutron attenuation coefficient (Sears, 1992). Some

Title Page

Abstract | Introduction

Conclusions | References

Tables | Figures

◄ | ►

◄ | ►

Back | Close

Full Screen / Esc

Printer-friendly Version

Interactive Discussion

neutrons therefore reach the detector from multiple scattering events with the sample and the instrument environment and this must be considered if the structure and fluid distribution is to be defined with high accuracy (Hassanein, 2006).

Neutron imaging is to great extent performed using acquisition systems based on a scintillator and a cooled precision camera equipped with either a CCD (Charge-Coupled Device) or a sCMOS (scientific Complementary Metal-Oxide Semiconductor) detector chip. The two technologies have their advantages respectively and complement each other. CCD chips have higher quantum efficiency and larger full well depth which makes them the better choice for long time exposures. In contrast the sCMOS has much shorter read-out time, allowing high frame rates with lower readout noise levels, making these the camera of choice for real-time experiments with very low neutron counts. These features make the camera type the better choice for real-time experiments. For selected applications amorphous silicon flat panel detectors are also suitable. At PSI the cameras are mounted in different camera boxes with adjustable focal distances and thus providing different the fields of view (FOV) dimensions. Three standard boxes with different dimensions provide FOV in the range of 15–300 mm with pixel sizes down to 6.5 µm.

When designing an experiment the key features to consider are the ability to resolve the feature of interest with sufficient resolution in time and space. The contrast also plays an important role and is directly related to the attenuation coefficient of the different components in the sample. In the end, the number of captured neutrons determines how well this contrast can be resolved. Mostly, the contrast in attenuation coefficient and the signal to noise ratio determines the detectability. Figure 1 shows the average number neutrons (N) that can be detected for different exposure times and pixel sizes for a neutron flux of 10^7 n cm^{-2} s^{-1}. The signal to noise ratio (SNR) is related to the neutron count as $\sqrt{N}$ as the noise can be described by a Poisson distribution. The scaling of the number of captured neutrons to the grey levels presented in the images varies with the detection system, i.e. which scintillator-lens-camera combination that was used.

2.1 Neutron imaging with high spatial resolution

~~The~~ high-resolution neutron imaging has been identified as one of the major demands of neutron imaging user community <mark>from which a number of scientific domains are foreseen to profit.</mark> While X-ray imaging can <mark>be nowadays performed</mark> routinely with micrometre spatial resolution even using table-top instrumentation, the spatial resolution of isotropic neutron imaging ~~that is routinely performed at major neutron imaging~~ is currently limited to deca-micrometre domain (Kaestner et al., 2011a; Williams et al., 2012; Tremsin et al., 2012). ~~The~~ single micrometre spatial resolution neutron imaging <mark>has been hitherto</mark> routinely available (in one direction) in the case of anisotropic imaging by Boillat et al. (2008). Apart from the <mark>above-mentioned</mark> instruments, there are hybrid detectors that <mark>apparently</mark> allow for sub-10 µm spatial resolution of neutron imaging, however their performance is currently rather limited regarding their temporal resolution (J. Jakubek, Detector performance, personal communication, 2015). Likewise, ~~it is necessary to mention here~~ the development of achromatic neutron microscope based on axisymmetric focussing mirrors (so-called Wolter optics) ~~that~~ promise ~~possible~~ "dramatic improvements in the signal rate and (spatial) resolution" (Liu et al., 2013). However, the current resolution of cold-neutron Wolter optics is limited to ~~many~~ deca-micrometres. A recent addition to the collection of high resolution neutron imaging systems is a microscope developed within the "Neutron Microscope project" at PSI. The first prototype of the microscope (Neutron Microscope 1.01) magnifies the image based on a 4 µm thick gadolinium oxysulfide (Gd2O2S:Tb) scintillator screen onto a high-resolution pixelated detector by a factor of 4.3. Thanks to this magnification factor, the pixel size of the neutron images based on the Neutron Microscope 1.01 could have reached 1.5 µm and the true spatial resolution of the resulting images has been recently reported to be equal to 7.6 µm (Trtik et al., 2015). The improvement in the spatial resolution over the standardly used test-setup for high resolution at PSI (Kaestner et al., 2011a) can be readily compared from the images of the test object (gadolinium

Siemens star) shown in Fig. 2a and b. The acquisition time for the image shown in Fig. 2 has been approximately 25 min.

2.1.1 High-resolution neutron imaging of drying of a model sample of porous medium

⁵ Despite the necessity of relatively long acquisition times needed for the imaging with Neutron Microscope prototype 1.01, the instrument allows for the observation of slow processes in radiographic mode.

In order to demonstrate the spatio-temporal capabilities of the Neutron Microscope prototype 1.01, a sample of a model porous medium has been created and investigated ¹⁰ at BOA beamline.

The sample consists of SiO_2 capillary (of 1.25 and 1.0 mm inner and outer diameter respectively) and stainless steel spheres of about 1.0 mm in diameter. The model porous medium sample was initially saturated with H_2O and the water was then left evaporating freely from the sample in-situ at ambient environment. The field of view ¹⁵ is equal to approximately 3 mm × 3 mm and the pixel size of the images was equal to 6 μm pixel size (i.e. 4× binning in both directions). The time-series revealed the removal of water from the pore space and the build-up of water menisci at the solid-solid boundaries over the time span of more than 6 h. The individual acquisition times were equal to 90 s (i.e. three times 30 s). Every 10th image from this data series (i.e. the time ²⁰ gap between individual images is equal to 15 min) is shown in Fig. 3. Slightly darker trapezoidal object at the bottom of the field of view represents, predominantly, the hydrogenous material in the adhesive of the aluminum tape that was used for the sample fixation. The presented time series demonstrates that processes occurring in porous media can be investigated with high spatial resolution in 2-D. This result give hope that ²⁵ also a 3-D high resolution neutron imaging of slow processes can be performed. We foresee that the advanced reconstruction methods (that can rely on the knowledge of the "initial" stationary stage of the porous medium, cf. Sect. 2.3) can be successfully utilized.

Neutron imaging for porous media

A. Kaestner et al.

Title Page

Abstract | Introduction

Conclusions | References

Tables | Figures

◄ | ►

◄ | ►

Back | Close

Full Screen / Esc

Printer-friendly Version

Interactive Discussion

2.2 Real-time neutron CT 💬

The nature of fluids makes it relevant to perform imaging experiments that observe a dynamic process through time. Approaches vary with the required contrast, spatial resolution, and the temporal development of the observed process. The main challenge during a real-time CT experiment is to avoid motion artefacts. These artefacts appear when the sample changes in shape or material distribution over the duration of an individual CT scan. Displacements of even a few percent of the pixel size can cause motion artefacts in the reconstructed data. These artefacts appear as tangential streaks emerging from the changing region. Real-time neutron CT is not necessarily artefact free, but it should have sufficient temporal resolution that any artefacts that appear do not impact the ability to follow the process or evaluate the data. In some circumstances increasing acquisition speeds may reduce image blur, but it can be counterproductive as the image quality is substantially reduced by lower SNR and possibly coarser resolution.

2.2.1 High dynamic range and spatial resolution

High spatial resolution imaging with sufficient contrast to detect small changes in the fluid distribution require longer exposure times to obtain sufficient neutron statistics. The exposure times of several tens of seconds or even minutes per projection are not uncommon with neutron imaging. Thus, CT scan durations in the order of several hours are not uncommon. Increasing the amount of neutrons improves the level of detail in the contrast, and the signal to noise ratio is increased: thus improving the probability of detection, and reducing the errors in qualitative and quantitative analysis of fluid distribution. For most aqueous processes, significant changes in the fluid distribution are likely even in the the duration of a single exposure, and motion artefacts in the reconstructed data are therefore significant. Two methods to reduce the impact of these artefacts use acquisition sequences that repeat the same acquisition angle several times during the scan, and output the change in the sample as a gradient from the

Title Page

Abstract | Introduction

Conclusions | References

Tables | Figures

◄◄ | ►►

◄ | ►

Back | Close

Full Screen / Esc

Printer-friendly Version

Interactive Discussion

greatest to the smallest extent of the dynamic region (Kaestner et al., 2011b). The first approach uses the repetition of several scans with equiangular increments each with a slight angular offset upon start. The second uses angular increments determined by the golden ratio as introduced by Köhler (2004). The latter method is more flexible since the golden ratio generates an infinite series of angles, and can be stopped at any time.

The major advantage of these alternative acquisition sequences is that they can be decomposed into shorter sub-scans (i.e. each scan uses a subset of the total projections collected) therefore producing a time-series of CT data from a single acquisition session. The time interval of each 3-D image (i.e. the number of projections used to reconstruct a single 3-D image) can be selected after the experiment as the exact start point and time scale of the phenomena in a specific sample does not need to be known ahead of the experiment. The time scale of the reconstructed data can be tuned at reconstruction time by selecting an adequate subset of projections. Techniques for reconstructing this kind of data and an example with experiment data are described in Sect. 2.3 below.

2.2.2 Rapid acquisition

When the process of interest is rapid, it is not possible to use the acquisition schemes described in the previous section, as there is still too much change in each individual projection. Under these conditions the acquisition frame rate must be increased at the cost of neutron statistics. The consequence is that dynamic range of the gray levels and SNR will be inferior in the reconstructed data. The sCMOS cameras allow frame rates greater than 25 frames per second (making it possible to acquire an entire set of CT projection data in about ten seconds). This was demonstrated by Zarebanadkouki et al. (2015). However, the neutron statistics is the limiting factor for the success of the experiment, unless the pixel size is increased (Fig. 1). Pixel size increases can be achieved either by binning on the camera side or by increasing the focal distance of the lens which will increase the field of view. Both ways will reduce the spatial resolution of the images. Low SNR in the projection data increase the importance of high quality

Neutron imaging for porous media

A. Kaestner et al.

Title Page

Abstract | Introduction

Conclusions | References

Tables | Figures

◄ | ►I

◄ | ►

Back | Close

Full Screen / Esc

reference data. The lower average neutron count per pixel in the image means the more reference images are needed to avoid contamination of the projection data by the noise introduced by the open beam (flat/bright) and dark current (dark) images. In addition to the feasibilty given by the neutron statistics also the sample stability under
5 centrifugal forces of higher rotation speeds should also be considered. Therefore, the acquisition rate must be determined as a balance between the boundary conditions given by instrument and sample.

As example for the rapid acquisition option, we have chosen the study of water uptake in roots. Rate and location of root water uptake by plants growing in soil has been
10 little understood due to the dynamic behaviour of soil and roots of transpiring plants. In this experiment, the water uptake by the roots of a small Lupine plant was studied. Neutron radiography was successfully used to overcome this difficulty thanks to its high spatio-temporal resolution and as well as its high sensitivity to deuterated water (D_2O) which has similar physical properties as those of water (Zarebanadkouki et al., 2012,
15 2014). The root uptake was quantified from data of D_2O redistribution within root using a diffusion convection model. The authors claimed that their method and its involved assumptions could be improved by three-dimensional imaging of D_2O transport in the root that will open new possibilities to address long standing questions such as relative importance of the apoplastic and cell-to-cell pathways of water across the root. Such
20 a tomography is challenging due to required high temporal resolution as the replacement of H_2O with D_2O within the root has been proven to be fast (a course of several minutes). Note that in particular a high spatial resolution was needed due to reduce motion artefacts. Here, we used an on-the-fly tomography with spatial resolution of 45 µm and temporal resolution of two CT scans per minute to monitor D_2O transport into the
25 roots of 14 days old lupines. Plants were grown in a cylindrical container (a diameter of 27 mm and a length of 100 mm) filled with a sandy soil. The neutron tomography was performed at the beamline ICON at the Paul Scherrer Institute (PSI), Villigen, Switzerland. We used an Andor NEO sCMOS camera set to a field of view of 55 mm × 116 mm (1200 × 2560 pixels) to capture 2-D neutron radiographs. To reconstruct 3-D volumet-

ric information 181 projections were acquired with uniform angluare increments over 180° with an exposure time of ca. 167 ms (1/6 s). It took about 30 s to capture the 181 projections needed for a CT. The sample was placed on a rotation stage that allows a continuous rotation of sample at a rotation rate of $\omega = 6° \, s^{-1}$. Compared to the experiments presented in Zarebanadkouki et al. (2015) this experiment used about 40 % of the neutrons per pixel (here about 100 neutrons pixel^{-1}) and provided a frame rate six times greater. The lower neutron count results in a lower SNR, but the image quality is still acceptable for the investigation. After capturing a first CT representing the steady state condition of the sample, D_2O was injected into the soil near the roots and its transport was simultaneously monitored using a time-series neutron radiograph.

Figure 4a shows a neutron radiograph of a 14 day old lupine before D_2O injection. This radiograph is taken at the initial position of the CT scan and shows the average neutron attenuation along the thickness of the sample. This image is normalized for flat field and camera dark current. We used 181 projections obtained by scanning the sample at the angular view from 0 to 180° to reconstruct the volumetric neutron attenuation in the sample. Figure 4b–d show a 2-D horizontal cross section at different depths of the sample. One of our concerns when short exposure times are used was whether the dynamic range was sufficient to distinguish between soil and roots. The experiment results did however show a reasonable contrast. After reconstruction, the root system could easily be segmented from the soil due to the high contrast in neutron attenuation between roots and soil (Fig. 4e).

Figure 5 shows selected 2-D horizontal cross section near the main root at a depth of 50 mm from the soil surface at different times after the D_2O injection. This figure shows the voxel-wise neutron attenuation within soil and root at different times as D_2O moves into the roots at night-time. The image sequence clearly show the radial transport of D_2O into the root. With time as D_2O moves into the root neutron attenuation decreases with a detectable gradient between the root periphery and its central parts. The reconstructed volumes were sufficiently accurate to quantify the changes of D_2O across the root tissue. This study proves that on the fly tomography can be successfully

used to study the flow of water across the root tissue in three dimensions at sufficiently high spatial and temporal resolution. The success in our 3-D visualization of D_2O transport across the root tissue opens new avenues to study the relative importance of the apoplastic and cell-to-cell pathways in root water uptake. Such information is urgently needed for understanding the physical mechanisms controlling water, solute and hormone transport in the roots.

2.3 Towards new reconstruction methods

Experimental projection data are usually reconstructed using the analytical filtered back projection (FBP) reconstruction algorithm Buzug (2008), which requires a large number of projections to perform well (i.e. to fullfil the sampling theorem). FBP is also sensitive to inaccuracies in the measured projection data. This can be a major problem when increasing acquisition speed for higher temporal resolution. Under-sampled projection data is best treated using iterative reconstruction techniques, as these can account for various inaccuracies in measurements and impose some regularity (e.g. smoothness) on the seeking solution. Normally, a priori information assumes some expected local intensity correlations, i.e. regions that remain unchanged throughout the experiment. The knowledge of initial stationary "dry" stage in the fluid-flow problem can be used as a prior reference for reconstruction. Several techniques which employ information of the "dry" stage were recently proposed Van Eyndhoven et al. (2015). For the sake of the visual comparison we provide under-sampled axial slice reconstructions (size 1000 × 1000 pixels) using 60 projections acquired at angles given by the golden ratio firing order, cf. Sect. 2.2.1. The slices were reconstructed using four different methods (see Fig. 6). The experiment data was collected at ICON (PSI) and represents a rock sample with a fluid in the pore space. It can be seen that CGLS-NLST method Kazantsev et al. (2015a) gives significantly better resolution than other techniques. The reconstructed image has also less streak artifacts caused by the under-sampled and better noise characteristics since regularization is driven by the pre-reconstructed "dry" image (see

Fig. 7). Initially, the stationary reference image is reconstructed from 150 projections using CGLS-TV algorithm.

By reconstructing ~~the~~ smaller projection subsets of the time-evolving projection data it is possible to demonstrate time-lapse series of the liquid ingress in the porous me-
5 dia (see Fig. 8). with the improved feature resolution after CGLS-NLST reconstruction (Kazantsev et al., 2015a), the liquid volumes can be quantified.

Another successful approach for reconstruction of under-sampled time-lapse pro-jection data of liquid distribution in solid stationary sample is given in Van Eyndhoven et al. (2015). The idea is to impose prior information by segmenting the reconstructed
10 stationary stage (i.e. extracting the rock phase) and then iteratively refine two other phases (air and liquid) by applying known intensity constraints Kazantsev et al. (2015a, b); Van Eyndhoven et al. (2015). The rock phase is also updated in iterations through comparison of measured and estimated projection data. This approach gives much better spatio-temporal resolution than has been previously achieved Kazantsev et al.
15 (2015a, 2014), however it is more parametrized and data-dependent.

2.4 Bimodal imaging – combining neutron and X-ray imaging

Every imaging modality has it strengths and weaknesses and one method is not always capable of providing all the information needed to understand sample behaviour. This is the case when a second modality can be used to complement the investigation to add
20 further information about the sample composition. Combining neutron and X-ray CT is one bimodal example particularly relevant for investigations of processes ~~on the pore scale~~ in porous media. The attenuation coefficients of both modalities are significantly different, therefore multivariate methods will provide better results than using single data sources. In some cases the contrast is even reversed between the modalities,
25 e.g. water which is low contrast for X-rays while it provides a high contrast for neutrons. There are two typical use cases for bimodal imaging: (1) the sample is static but it is difficult to identify relevant features due to small differences in contrast and (2) samples with a dynamic component. In the latter case one modality can be used to identify

the static structures while the other is used to capture the displacements caused by the observed process. A combination of the two approaches can off course also be beneficial.

The bimodal imaging concept using neutrons and X-rays is adopted and available to users at NEUTRA (Mannes et al., 2015; Vontobel et al., 2015) and will be operational in a near future at ICON (Kaestner et al., 2015). These beamlines are equipped with X-ray sources that make it possible to obtain both neutron and X-ray images without moving the sample from the sample position and perform experiments with either simultaneously or interleaved (one modality after the other) bi-modal acquisition. A further advantage of using the same sample manipulation environment reduce the registration efforts to align the image data from the modalities on a common coordinate system. This is in particular true for the installation at NEUTRA where the X-ray source is mounted to provide very similar beam geometry as the neutron beam. This make pixel wise comparisons possible. At ICON, a different approach has been chosen with a divergent X-ray source with the X-ray beamline mounted perpendicular to the neutron beam direction. This installation has the advantage that time is minimized between the acquisition using each modality.

There are several strategies to analyze the bi-variate data. The work flow is however usually initiated by a registration step to align the data sets on a common coordinate system. This will guarantee a pixel/voxel-wise combined analysis of the two data sets. There are approaches to start the data fusion already at the reconstruction stage which would require registration of the projection data. In other approaches the CT data is reconstructed separately to be fused at a later point in time. This is still work in progress. The choice of modality fusion strategy will depend on the sample type and the information to extract from the experiment.

As an example of combined X-ray and neutron tomography imaging we present the study of water and air behavior in soil. The infiltration of water and air trapping was studied on intact sample of coarse sandy loam soil (Cambisol series) from mountainous region of the Czech Republic taken in the depth of 40 cm below surface. The soil is

|◄ | ►|

◄ | ►

Back | Close

Full Screen / Esc

Printer-friendly Version

Interactive Discussion

known for the occurrence of the preferential flow (Dohnal et al., 2012), in which majority of water flux is conducted through small fraction of the soil volume mainly through soil macropores and other highly conductive structures. The preferential flow can be numerically simulated by dual-continuum models (e.g. Gerke et al., 2007), but current

5 models do not account for trapped air that can efficiently block the macropores and significantly reduce soil permeability for water (Snehota et al., 2015), thus model predictions are failing. The experiment performed at the NEUTRA beamline consisted of two infiltration episodes during which a layer of D_2O/H_2O mixture (in the approx. mass ratio of 95 : 5) was maintained on the sample surface (condition known as ponding),

10 while water was left to drain the sample freely through the bottom by gravity. Flooding of the sample surface and maintaining the water level was controlled remotely. One X-ray and two neutron tomograms of the sample in its initial state were performed before beginning of the first infiltration. Another 20 neutron tomograms were acquired during the following 25 h of the experiment (see selected tomograms in Fig. 9).

15 The neutron and X-ray tomograms were reconstructed by the MuhRec3 code (Kaestner, 2011) using 201 projections. The detector used for neutron imaging was a 100 µm thick LiF/ZnS scintillator screen photographed by a CCD camera (Andor iKON L BW936). The exposure time for each projection was 8 s and the acquisition time for one tomogram was aprox. 50 min. The image matrix size was 1024 × 1024 pixels and

20 the nominal pixel size was 0.101 mm × 0.101 mm. Fine co-registration of the X-ray and neutron tomograms was done by searching for the minimum of sum of differences while rotating and translating the X-ray tomogram as a rigid body. Bi-variate histograms shown in Fig. 10 helped to identify the threshold of 14 500 a.u. that was subsequently used for segmentation of the macropores from the X-ray tomogram.

25 The segmented X-ray tomogram was then used as a binary mask (see Fig. 11) to measure the water volume in macropores using neutron tomograms. Volume of water and subsequently the average water content in the macropore system was calculated by subtracting tomogram of the dry sample before the experiment and dividing the voxel values by attenuation coefficient of water. Figure 11b then shows the extent of the water

content reduction during the second infiltration due to air trapping quantitatively. The data are being used to further develop the follow-up model by Fucik et al. (2010) that is based on the two-phase flow approach.

3 Conclusions

We have shown that with today's instrumentation at state-of-the-art neutron imaging beamlines it is possible to observe processes in porous media in a similar scale in time and space as lab based X-ray sources. With the high sensitivity to hydrogen, neutron imaging is the ideal probe for high resolving multidimensional experiments with the objective to investigate the distribution of fluids in porous media. Our instrumentation options make it possible to obtain spatial resolutions of a few micrometres and CT volume rates of a couple volumes per minute with pixel sizes of about 50 µm. Yet, often this achieved at a the cost of lower signal to noise ratio than known from the X-ray based imaging systems. The presented use cases show to what extent new experiment equipment and numerical methods make new insights possible using neutron imaging. While it is important that the data can be acquired, there is an important task after the experiment to prepare and analyze the data. The techniques shown here are aiming at obtaining information on the limits what the beam can provide. This requires special attention to the analysis compared to the comfortable case of well exposed data, this is a topic about to be addressed in the near future. The neutron imaging community is currently in the early stages of developing improved methods to analyse multidimensional data beyond the third dimension and/or multimodal data under low SNR conditions. A close collaboration between user community, instrument scientists, and algorithm developers is required to fully be able to extract all relevant information in the measured data. For experiments that produce data with intrinsic time structure it is often beneficial to perform the analysis in 4-D instead as processing the data as a sequence of 3-D images. This is for exeample the approach used for the spatio-temporal reconstruction technique described Sect. 2.3. Ideally, the following analysis

~~steps~~ should also involve the time structure in the data with the benefit of more accurate <mark>analysis.</mark>

<mark>With new developed methods and the possibilities provided by new technology,</mark> neutron imaging is good choice to observe and quantify transport processes in porous media at different scales in time and space, <mark>regardless</mark> whether the pore space can be resolved or not.

References

Boillat, P., Kramer, D., Seyfang, B., Frei, G., Lehmann, E., Scherer, G., Wokaun, A., Ichikawa, Y., Tasaki, Y., and Shinohara, K.: In situ observation of the water distribution across a PEFC using high resolution neutron radiography, Electrochem. Commun., 10, 546–550, doi:10.1016/j.elecom.2008.01.018, 2008. 3485

Buzug, T.: Introduction to Computed Tomography: From Photon Statistics to Modern Cone-Beam CT, Springer, 2008. 3491

Dohnal, M., Vogel, T., Sanda, M., and Jelinkova, V.: Uncertainty analysis of a dual-continuum model used to simulate subsurface hillslope runoff involving oxygen-18 as natural tracer, J. Hydrol. Hydromech., 60, 194–205, doi:10.2478/v10098-012-0017-0, 2012. 3494

Fucik, R., Sakaki, J. M. T., Benes, M., and Illangasekare, T.: Significance of dynamic effect in capillarity during drainage experiments in layered porous media, Vadose Zone J., 9, 697–708, doi:10.2136/vzj2009.0106, 2010. 3495

Gerke, H., Dusek, J., Vogel, T., and Kohne, J.: Two-dimensional dual-permeability analyses of a bromide tracer experiment on a tile-drained field, Vadose Zone J., 6, 651–667, doi:10.2136/vzj2007.0033, 2007. 3494

Full Screen / Esc

Printer-friendly Version

Interactive Discussion

Hassanein, R.: Correction methods for the quantitative evaluation of thermal neutron tomography, Diss. eth no. 16809, Swiss Federal Institute of Technology, 2006. 3484

Kaestner, A.: MuhRec – a new tomography reconstructor, Nucl. Instrum. Meth. A, 651, 156–160, doi:10.1016/j.nima.2011.01.129, 2011. 3494

5 Kaestner, A., Hartmann, S., Kuehne, G., Frei, G., Gruenzweig, C., Josic, L., Schmid, F., and Lehmann, E.: The ICON beamline – a facility for cold neutron imaging at SINQ, Nucl. Instrum. Meth. A, 659, 387–393, doi:10.1016/j.nima.2011.08.022, 2011a. 3483, 3485, 3501

Kaestner, A., Münch, B., Trtik, P., and Butler, L.: Spatio-temporal computed tomography of dynamic processes, Opt. Eng., 50, 123201, doi:10.1117/1.3660298, 2011b. 3488

10 Kaestner, A., Morgano, M., Hovind, J., and Lehmann, E.: Bimodal imaging using neutrons and X-rays, in: Proceedings of the International Symposium on Digital Industrial Radiology and Computed Tomography, Digital Industrial Radiology and Computed Tomography (DIR 2015), 22–25 June 2015, Belgium, Ghent, ndt.net, available at: http://www.ndt.net/?id=18061 (last access: 26 November 2015), 2015. 3493

15 Kazantsev, D., Van Eyndhoven, G., Lionheart, W. R. B., Withers, P. J., Dobson, K. J., McDonald, S. A., Atwood, R., and Lee, P. D.: Employing temporal self-similarity across the entire time domain in computed tomography reconstruction, Philos. T. R. Soc. A, 373, 2043, doi:10.1098/rsta.2014.0389, 2014. 3492

Kazantsev, D., Eyndhoven, G. V., Lionheart, W., Withers, P., Dobson, K., McDonald, S.,
20 Atwood, R., and Lee, P.: Employing temporal self-similarity across the entire time domain in computed tomography reconstruction, Philos. T. R. Soc. Lond., 373, 1–14, doi:10.1098/rsta.2014.0389, 2015a. 3491, 3492

Kazantsev, D., Thompson, W. M., Lionheart, W. R. B., Eyndhoven, G. V., Kaestner, A. P., Dobson, K. J., Withers, P. J., and Lee, P. D.: 4D-CT reconstruction with unified spatial-temporal
25 patch-based regularization, Inverse Probl. Imag., 9, 20, doi:10.3934/ipi.2015.9.447, 2015b. 3492

Köhler, T.: A projection access scheme for iterative reconstruction based on the golden section, in: Nuclear Science Symposium Conference Record, IEEE, 16–22 October 2004 Rome, Italy, vol. 6, 3961–3965, doi:10.1109/NSSMIC.2004.1466745, 2004. 3488

30 Lehmann, E., Kaestner, A., and Mannes, D. (Eds.): Proceedinings of the 10th World Conference on Neutron Radiography, Paul Scherrer Institute, Physics Procedia, Elsevier Science Publishers, Grindelwald, Switzerland, 2015.

Neutron imaging for porous media

A. Kaestner et al.

Title Page

Abstract | Introduction

Conclusions | References

Tables | Figures

◄ | ►

◄ | ►

Back | Close

Full Screen / Esc

Printer-friendly Version

Interactive Discussion

Lehmann, E. H., Vontobel, P., and Wiezel, L.: Properties of the radiography facility NEUTRA at SINQ and it's potential for use as European reference facility, Nondestruct. Test. Eva., 16, 191–202, doi:10.1080/10589750108953075, 2001. 3483

Liu, D., Hussey, D., Gubarev, M. V., Ramsey, B. D., Jacobson, D., Arif, M., Moncton, D. E., and Khaykovich, B.: Demonstration of achromatic cold-neutron microscope utilizing axisymmetric focusing mirrors, Appl. Phys. Lett., 102, 183508, doi:10.1063/1.4804178, 2013. 3485

Mannes, D., Schmid, F., Frey, J., Schmidt-Ott, K., and Lehmann, E.: Combined Neutron and X-ray imaging for non-invasive investigations of cultural heritage objects, in: Proceedinings of the 10th World Conference on Neutron Radiography, Paul Scherrer Institute, Physics Procedia, Elsevier Science Publishers, 653–660, 2015. 3493

Morgano, M., Peetermans, S., Lehmann, E., Panzner, T., and Filges, U.: Neutron imaging options at the BOA beamline at Paul Scherrer Institut, Nucl. Instrum. Meth. A, 754, 46–56, doi:10.1016/j.nima.2014.03.055, 2014. 3483

Sears, V.: Neutron scattering lengths and cross sections, Neutron News, 3, 26–37, doi:10.1080/10448639208218770, 1992. 3483

Snehota, M., Jelinkova, V., Sobotkova, M., Sacha, J., Vontobel, P., and Hovind, J.: Water and entrapped air redistribution in heterogeneous sand sample: Quantitative neutron imaging of the process, Water Resour. Res., 51, 1359–1371, doi:10.1002/2014WR015432, 2015. 3494

Tremsin, A., McPhate, J., Vallerga, J., Siegmund, O., Feller, W., Lehmann, E., Kaestner, A., Boillat, P., Panzner, T., and Filges, U.: Neutron radiography with sub-15 μm resolution through event centroiding, Nucl. Instrum. Meth. A, 688, 32–40, doi:10.1016/j.nima.2012.06.005, 2012. 3485

Trtik, P., Hovind, J., Grünzweig, C., Bollhalder, A., Thominet, V., David, C., Kaestner, A., and Lehmann, E. E.: Improving the spatial resolution of neutron imaging at Paul Scherrer Institut – The Neutron Microscope Project, in: Proceedinings of the 10th World Conference on Neutron Radiography, Paul Scherrer Institute, Physics Procedia, Elsevier Science Publishers, 2015. 3485, 3501
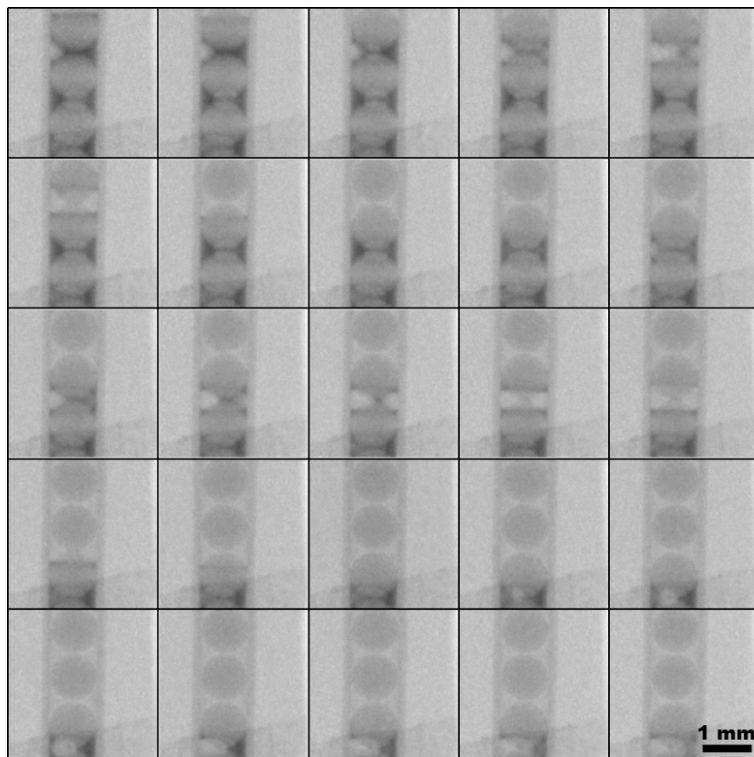
Van Eyndhoven, G., Batenburg, K., Kazantsev, D., Van Nieuwenhove, V., Lee, P., Dobson, K., and Sijbers, J.: An iterative CT reconstruction algorithm for fast fluid flow imaging, IEEE T. Image Process., 24, 4446–4458, doi:10.1109/TIP.2015.2466113, 2015. 3491, 3492

Vontobel, P., Mannes, D., Kaestner, A., Schmid, F., and Lehmann, E. H.: The X-ray option at the NEUTRA imaging beamline of the spallation neutron source SINQ, Nucl. Instrum. Meth. A, in review, 2015. 3493

Neutron imaging for porous media

A. Kaestner et al.

Title Page

Abstract	Introduction
Conclusions	References
Tables	Figures

◀◀ ▶▶

◀ ▶

Back Close

Full Screen / Esc

Printer-friendly Version

Interactive Discussion

Williams, S., Hilger, A., Kardjilov, N., Manke, I., Strobl, M., Douissard, P., Martin, T., Riese-
    meier, H., and Banhart, J.: Detection system for microimaging with neutrons, J. Instrum., 7,
    P02014, doi:10.1088/1748-0221/7/02/P02014, 2012. 3485

Zarebanadkouki, M., Kim, Y. X., Moradi, A. B., Vogel, H. J., Kaestner, A., and Carminati, A.:
    Quantification and modeling of local root water uptake using neutron radiography and deuter-
    ated water, Vadose Zone J., 11, doi:10.2136/vzj2011.0196 2012. 3483, 3489

Zarebanadkouki, M., Kroener, E., Kaestner, A., and Carminatis, A.: Visualization of root water
    uptake: quantification of deuterated water transport in roots using neutron radiography and
    numerical modeling, Plant Physiol., 166, 487–499, doi:10.1104/pp.114.243212, 2014. 3489

Zarebanadkouki, M., Carminati, A., Kaestner, A., Mannes, D., Morgano, M., Peetermans, S.,
    Lehmann, E., and Trtik, P.: On-the-fly neutron tomography of water transport into lupine roots,
    in: Proceedinings of the 10th World Conference on Neutron Radiography, Paul Scherrer
    Institute, Physics Procedia, Elsevier Science Publishers, doi:10.1016/j.phpro.2015.07.041,
    2015. 3488, 3490

Neutron imaging for porous media
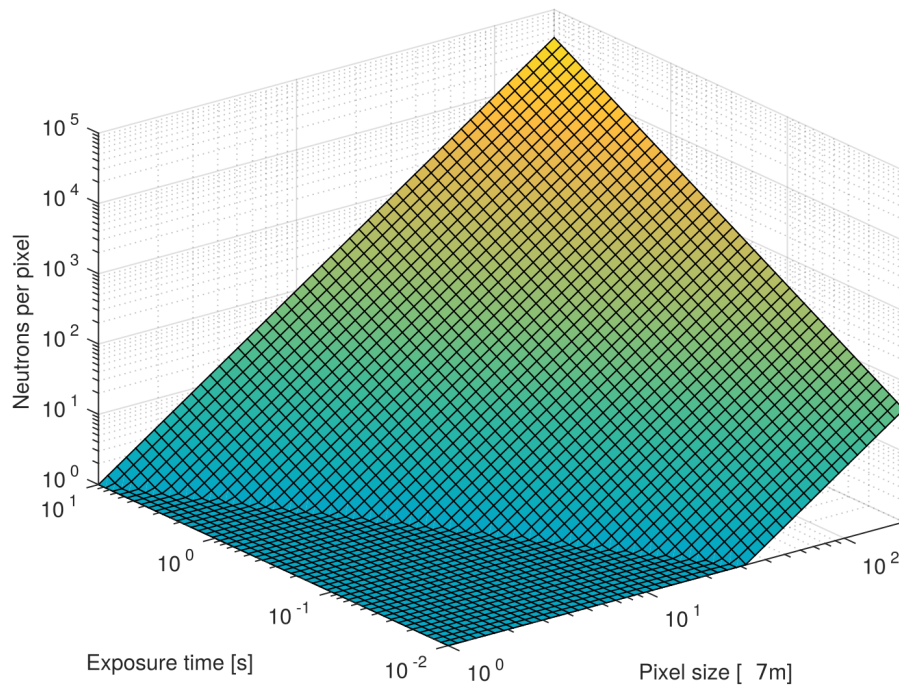
A. Kaestner et al.

Figure 1. Average number of neutrons per pixel as function of exposure time and pixel size calculated for a neutron flux of $10^7 \, \mathrm{n\,cm^{-2}\,s^{-1}}$.

Figure 2. Comparison of the neutron radiographs of gadolinium Siemens star test object based on **(a)** standard high-resolution neutron instrument (Kaestner et al., 2011a) and **(b)** the Neutron Microscope prototype 1.01 (Trtik et al., 2015).

Figure 3. Time-series (logically from-left-to-right and then from-top-to-bottom) of the evaporation of water from a model porous medium sample. The field of view is approximately $3\,mm \times 3\,mm$. The images with $6\,\mu m$ pixel size ($4\times$ binning) were acquired with $90\,s$ acquisition time. Only every 10th image is presented, therefore the time gap between the individual presented image is about $15\,min$.
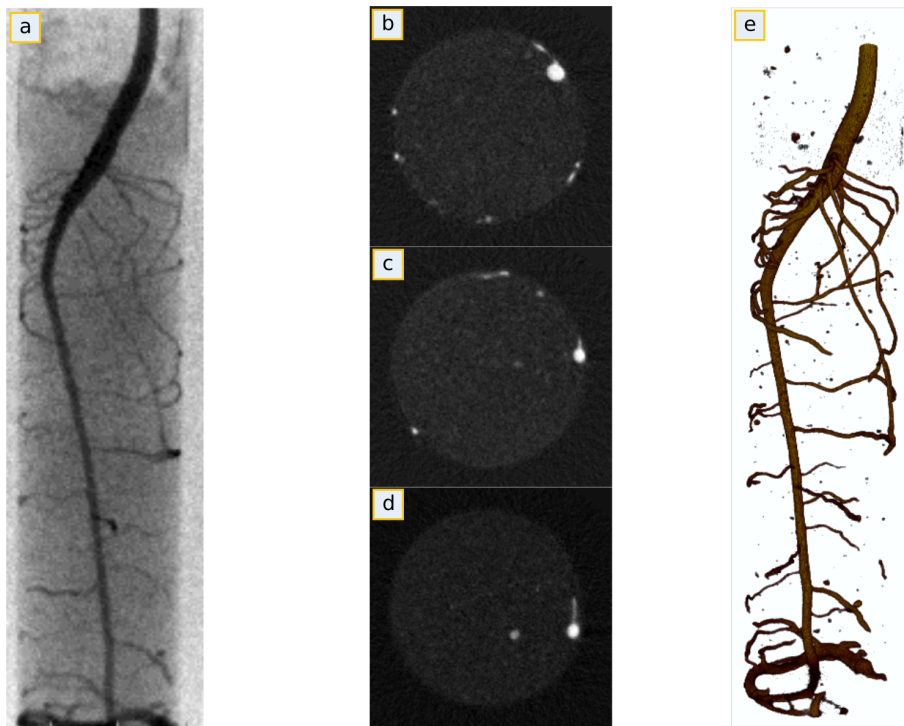
Figure 4. (a) Neutron radiography of a 2 weeks old lupine grown in a cylindrical container (a diameter of 27 mm and a length of 100 mm) filled with a sandy soil. **(b–d)** Horizontal cross section at different depths indicated by the black arrows. **(e)** There dimensional root system of the sample reconstructed using 181 projections taken at angular field of view from 0 to 180°.
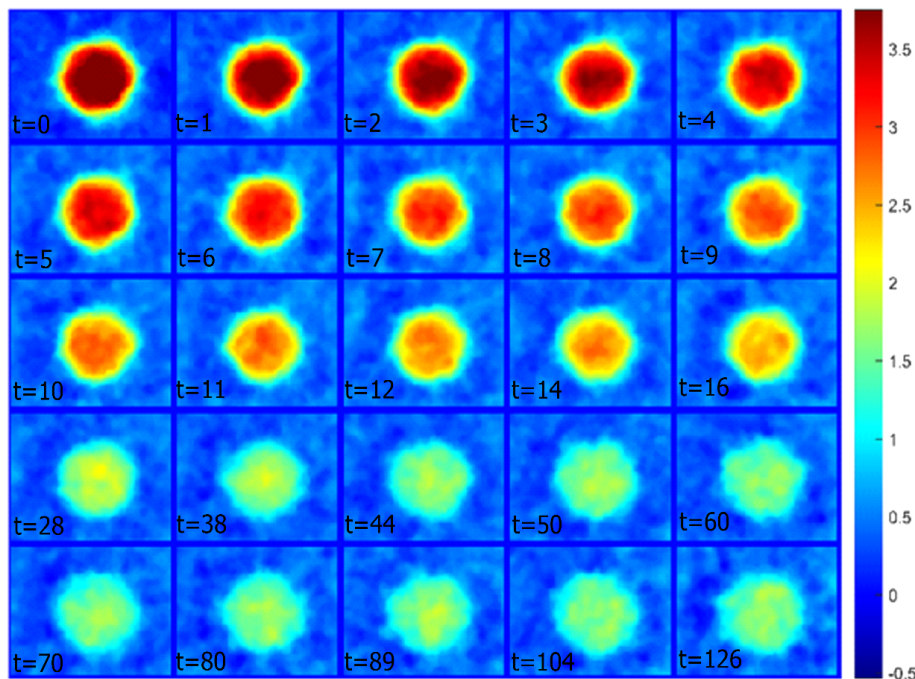
Figure 5. Time series neutron tomography of D_2O transport into the taproot of a two weeks old lupine during nighttime. These images show the change in neutron attenuation across the root tissue at different times after D_2O injection (time is indicated in minutes). As D_2O enters the root tissue the ratio of D_2O to H_2O increase and therefore the neutron attenuation decreases (blue color). The images show horizontal cross section at depth of 50 mm from soil surface and a close-up (5 mm × 5 mm) of the original field of view of 30 mm × 30 mm.
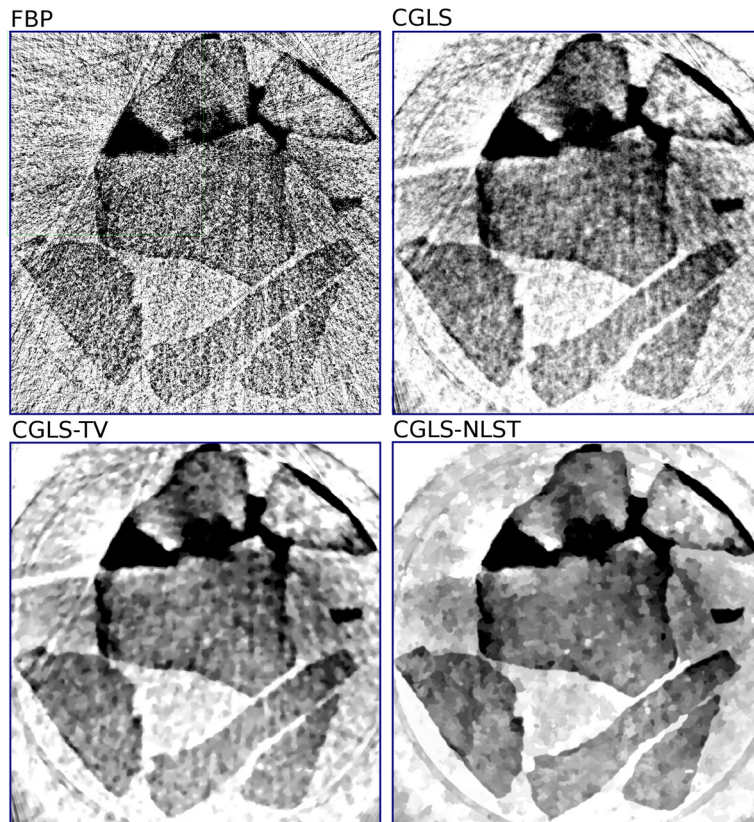
Figure 6. Reconstructed images with different methods showing the axial slices (1000 × 1000 pixels) of one time frame from the set of motion incorporated projections. The reconstructed time frame consists of 60 projections.
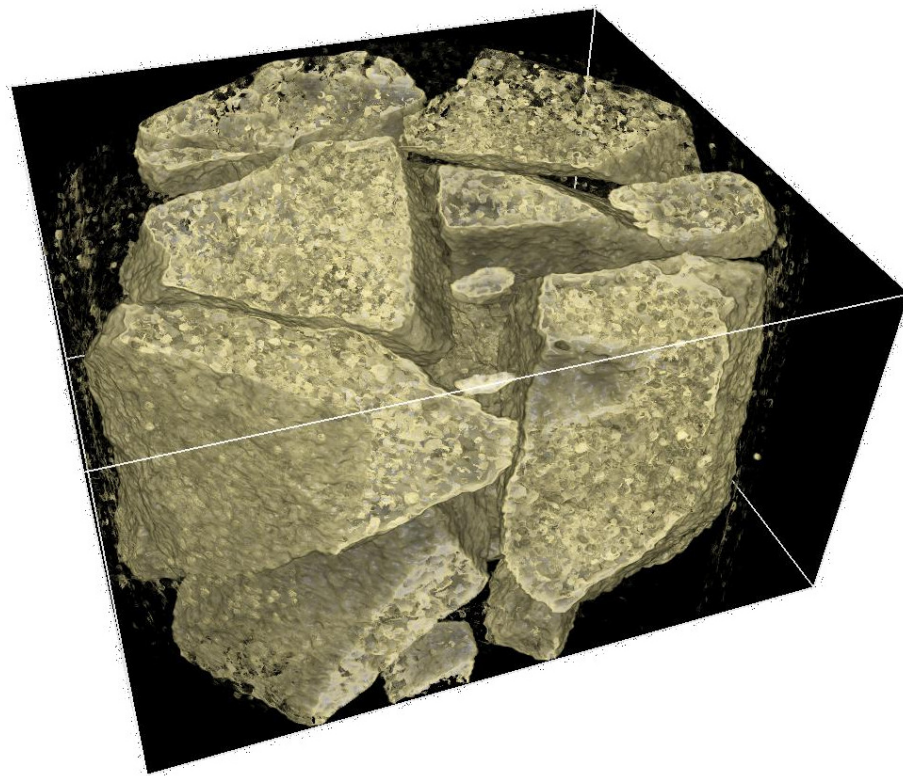
Figure 7. Rendered volume of the stationary "dry" sample (sandstone) prior to water ingress. Reconstruction from 150 projections using CGLS-TV algorithm.

Discussion Paper | Discussion Paper | Discussion Paper | Discussion Paper
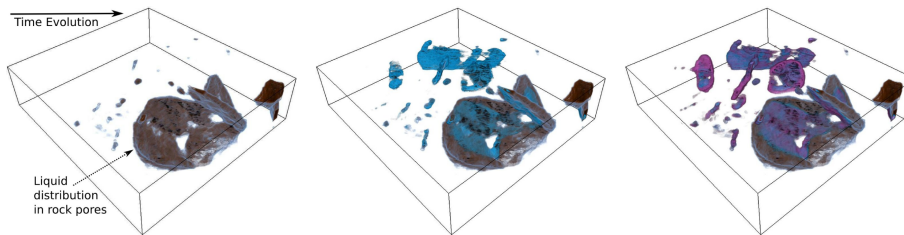
Figure 8. The fluid phase in the rock sample at three different times of the water ingress. Each volume is reconstructed from 60 projections using the CGLS-NLST method.
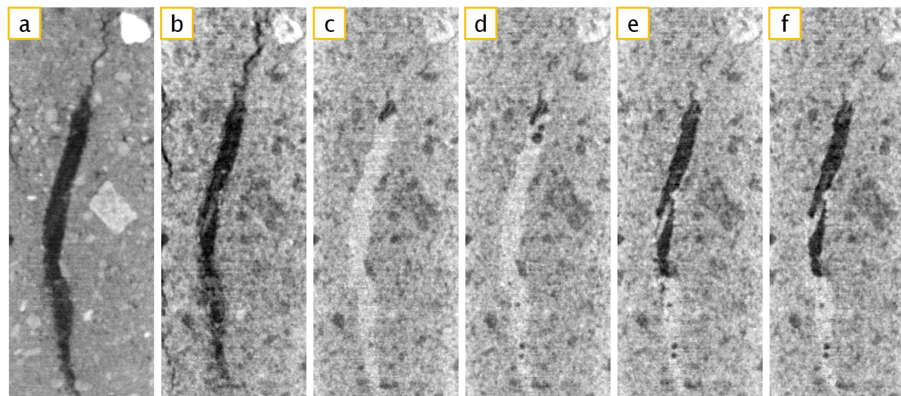
Figure 9. Cropped part (22.1 mm × 60.0 mm) of the vertical cross sections through X-ray **(a)** and neutron tomograms **(b, c)** of the intact soil sample taken into a cylinder (a diameter of 34 mm, height of 87 mm) during various stages of the recurrent ponded infiltration experiment: **(a, b)** before experiment when the macropore in the center of the image is filled with air, **(c)** during the infiltration when the macropore is entirely filled with water, **(d)** during continuing infiltration **(e)** after draining the sample, **(f)** during second infiltration episode when the entrapped air formed in the macropore.

Title Page

Abstract | Introduction

Conclusions | References

Tables | Figures

|◄ | ►|

◄ | ►

Back | Close

Full Screen / Esc

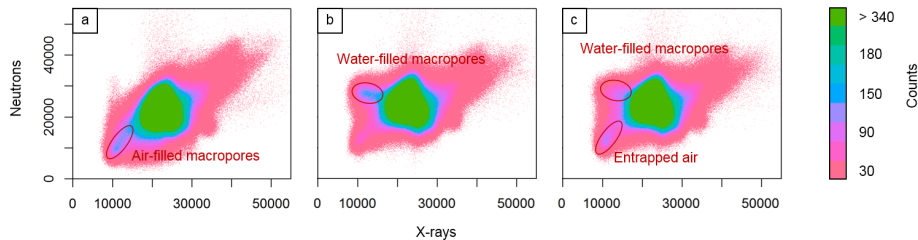Printer-friendly Version

Interactive Discussion

Figure 10. Bi-variate histograms of cropped part of the X-ray and corresponding neutron tomograms representing soil sample with large macropore during various stages of recurrent ponding infiltration experiment. Histograms show **(a)** empty macropore before the infiltration was started, **(b)** filling of the macropores during the first infiltration and **(c)** partial filling of the macropores during the second infiltration.
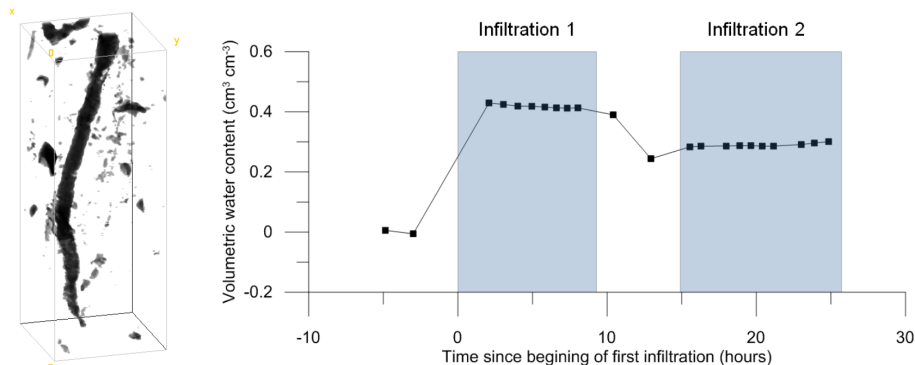
Figure 11. Macropore system that represents 1.97 % of the sample volume segmented from X-ray tomogram. (Right) Time sequence of water contents in the macropore system derived from series of 22 tomograms. The blue columns indicate the time of two ponding infiltration episodes.